Incommensurate and commensurate magnetic structures of the ternary germanide $CeNiGe_3$

2003 J. Phys.: Condens. Matter 15 77

(http://iopscience.iop.org/0953-8984/15/2/308)

INSTITUTE OF PHYSICS PUBLISHING JOURNAL OF PHYSICS: CONDENSED MATTER

J. Phys.: Condens. Matter **15** (2003) 77–90 PII: S0953-8984(03)40029-5

Incommensurate and commensurate magnetic structures of the ternary germanide $CeNiGe_3$

L Durivault[1,2], F Bourée[1], B Chevalier[2,4], G André[1], F Weill[2], J Etourneau[2], P Martinez-Samper[3], J G Rodrigo[3], H Suderow[3] and S Vieira[3]

[1] Laboratoire Léon Brillouin (CEA-CNRS), CEA/Saclay, 91191 Gif-sur-Yvette, France
[2] Institut de Chimie de la Matière Condensée de Bordeaux (ICMCB), CNRS (UPR 9048), Université Bordeaux I, 87 Avenue du Dr A Schweitzer, 33608 Pessac, France
[3] Universidad Autonoma de Madrid, Facultad de Ciencias, C-III Cantoblanco, 28049 Madrid, Spain

E-mail: chevalie@icmcb.u-bordeaux.fr

Received 29 July 2002
Published 20 December 2002
Online at stacks.iop.org/JPhysCM/15/77

Abstract

The structural properties of $CeNiGe_3$ have been investigated via electron diffraction and neutron powder diffraction (NPD). This ternary germanide crystallizes in the orthorhombic $SmNiGe_3$-type structure ($Cmmm$ space group). Electrical resistivity, ac- and dc-magnetization measurements show that $CeNiGe_3$ orders antiferromagnetically below $T_N = 5.5(2)$ K and exclude the occurrence at low temperatures of a spin-glass state for $CeNiGe_3$ as previously reported. Specific heat measurements and NPD both reveal two magnetic transitions, observed at $T_{N1} = 5.9(2)$ K and $T_{N2} = 5.0(2)$ K. Between T_{N1} and T_{N2}, the Ce magnetic moments in $CeNiGe_3$ are ordered in a collinear antiferromagnetic structure associated with the $\boldsymbol{k}_1 = (100)$ wavevector and showing a relationship with the magnetic structure of the $Ce_3Ni_2Ge_7$ ternary germanide. Below T_{N2}, this $\boldsymbol{k}_1 = (100)$ commensurate magnetic structure coexists with an incommensurate helicoîdal magnetic structure associated with $\boldsymbol{k}_2 = (0\ 0.409(1)\ 1/2)$. This last magnetic structure is highly preponderant below T_{N2} (93(5)% in volume). At 1.5 K, the Ce atoms in $CeNiGe_3$ carry a reduced ordered magnetic moment (0.8(2) μ_B). This value, smaller than that obtained in $Ce_3Ni_2Ge_7$, results from an important hybridization of the 4f(Ce) orbitals with those of the Ni and Ge ligands.

[4] Author to whom any correspondence should be addressed.

0953-8984/03/020077+14$30.00

1. Introduction

The $CeTGe_3$ ternary germanides, where T is a transition element such as Fe [1], Co [2, 3], Rh or Ir [4, 5], crystallize in the tetragonal $BaNiSn_3$-type structure. These compounds exhibit interesting physical properties resulting from two competing interactions:

(i) the Kondo interaction leading to a compensation of the Ce localized magnetic moments through the exchange interaction between the 4f(Ce) electrons and conduction electrons and
(ii) the Ruderman–Kittel–Kasuya–Yoshida (RKKY) interaction that plays an important role in establishing magnetic ordering in rare earth intermetallics.

$CeFeGe_3$ is then a 'moderate' heavy-fermion system ($\gamma \cong 150$ mJ mol^{-1} K^{-2}) with a high Kondo temperature ($T_K \cong 100$ K) [1]. $CeCoGe_3$ presents both heavy-fermion character ($\gamma \cong 111$ mJ mol^{-1} K^{-2}) and a complex magnetic phase diagram where two ordering temperatures, 21 and 18 K, are distinguished [2]. In contrast, the Kondo effect weakly influences the physical properties of $CeRhGe_3$ and $CeIrGe_3$, which both also show complex magnetic phase diagrams with three magnetic transition temperatures [4].

Among the $CeTGe_3$ series, $CeNiGe_3$ presents original structural properties. Two crystal structures have been proposed for this ternary germanide: the cubic $Yb_3Rh_4Sn_{13}$-type structure with some atomic disorder between Ce and Ge [6] and the orthorhombic $SmNiGe_3$-type structure [7]. Some uncertainty also exists concerning the magnetic properties of $CeNiGe_3$ as Das *et al* [6] claim that the magnetic ordering observed below 4.2 K could be either antiferromagnetic or spin-glass type.

Recently, studying the Ce–Ni–Ge system, we have shown that the ternary germanides containing 50 at.% of Ge or more order antiferromagnetically at low temperature [8]. The transition temperature T_N decreases with Ge content in the series; for instance Ce_2NiGe_6 [8], $Ce_3Ni_2Ge_7$ [9] and $Ce_2Ni_3Ge_5$ [10, 11] respectively containing 66.7, 58.3 and 50 Ge at.% have Néel temperatures T_N respectively equal to 10.4, 7.2 and 5.1 K [10] or 4.8 K [11]. In order to correlate this decrease of the T_N-temperature to an increase of the influence of the Kondo effect, we determined the magnetic structure of $Ce_3Ni_2Ge_7$ [9] and $Ce_2Ni_3Ge_5$ [11]. This correlation seems to be effective as the ordered Ce magnetic moments in $Ce_3Ni_2Ge_7$ and $Ce_2Ni_3Ge_5$ are respectively equal to 1.98(2) and 0.4(1) μ_B at $T = 1.5$ K, revealing then the stronger influence of the Kondo effect on the physical properties of $Ce_2Ni_3Ge_5$.

We now extend our study on magnetic structures of $CeNiGe_3$. Via neutron powder diffraction (NPD), we have recently shown that this ternary germanide is orthorhombic, with $SmNiGe_3$-type structure [12]. Here we report on synthesis, transmission electron microscopy (TEM), electrical, magnetic and heat capacity measurements, together with NPD performed on $CeNiGe_3$.

2. Experimental details

A polycrystalline $CeNiGe_3$ sample was prepared by melting appropriate amounts of at least 99.9% purity elements under a purified argon atmosphere using a water-cooled copper crucible in a high-frequency furnace. The sample was turned and remelted several times to ensure homogeneity. Then, an annealing treatment was performed in an evacuated quartz tube at 1073 K for one month.

The annealed sample was checked by microprobe analysis using a Cameca SX-100 instrument. The analysis was performed on the basis of intensity measurements of Ce L α_1, Ni Kα_1 and Ge Kα_1 x-ray emission lines, which were compared with those obtained for

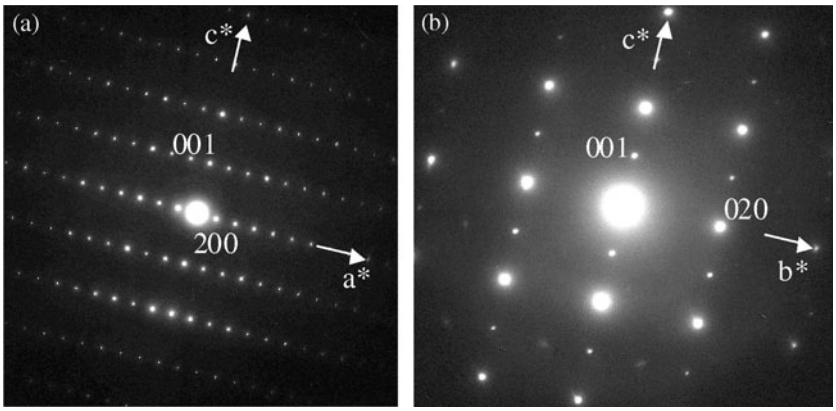

Figure 1. Selected-area electron diffraction patterns of $CeNiGe_3$ along the [010] (a) and [100] (b) zone axes.

CeNiGe used as reference compound. Our results show that is difficult to get a single phase; the main phase $CeNiGe_3$ coexists with some amount of Ge (<3–4% in mass). Let us note that Ge is a non-magnetic phase.

The electron diffraction investigation was carried out on a JEOL 2000FX microscope, operating at 200 kV, equipped with a double tilt specimen stage. For this experiment, the annealed sample was crushed in acetone and a drop of the suspension was deposited on a holey carbon support film. High resolution electron microscopy was performed on a piece of polycrystalline sample thinned by ion milling. Image simulation was performed using Cirius software.

Electrical resistivity was measured on a polycrystalline piece using a classical four-probe dc method. Magnetization data in an applied field up to 5 T were collected on a superconducting quantum interference device (SQUID) magnetometer. The heat capacity was measured by an adiabatic method in a ^{3}He refrigerator. The sample was fastened with a small amount of vacuum grease to a previously calibrated sample holder, and the temperature was measured using a calibrated RuO resistive thermometer. The contribution coming from the addenda (negligible below 6 K and increasing up to 30% at 14 K) was subtracted from the obtained measurement.

NPD patterns were collected using the two-axis diffractometers 3T2 (high resolution powder diffractometer; $\lambda = 0.1225$ nm) and G4-1 (800 cell-position-sensitive detector; $\lambda = 0.2426$ nm) at the Orphée reactor (CEA/Saclay, France). The data analysis was performed using the Fullprof program [13], with neutron scattering lengths and Ce^{3+} form factor taken respectively from [14] and [15].

3. Results and discussion

3.1. Structural properties

Figure 1 shows some selected-area electron diffraction patterns obtained on the $CeNiGe_3$ sample; the zone axis is [010] and [100], respectively for figures 1(a) and (b). These patterns are indexed on the basis of the orthorhombic $SmNiGe_3$-type (*Cmmm* space group, No 65) unit cell. The present study then confirms our $CeNiGe_3$ crystal structure determination from NPD [12].

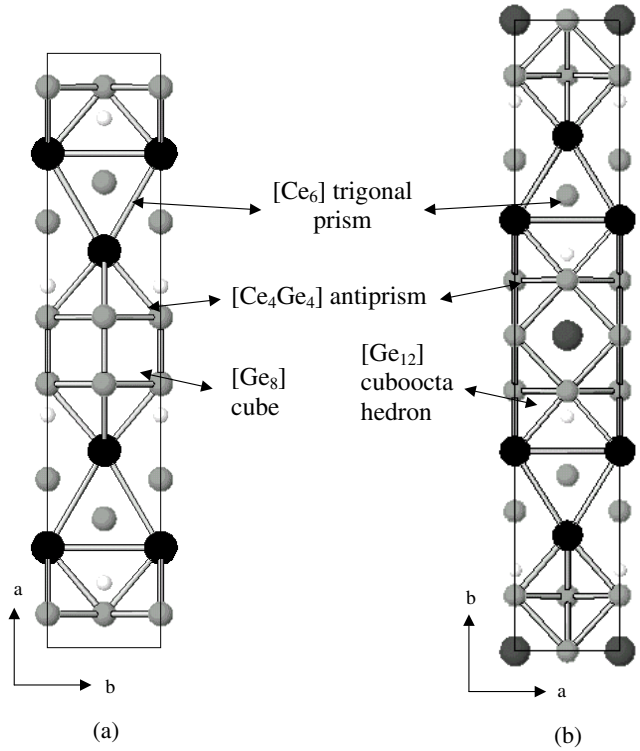

Figure 2. Structural relationship between $CeNiGe_3$ and $Ce_3Ni_2Ge_7$. Projection onto the 001 plane of the crystal structure of (a) $CeNiGe_3$ and (b) $Ce_3Ni_2Ge_7$. (Ce, Ge and Ni are respectively represented by large black, medium grey and small white circles.) The solid line represents the unit cell limits. We have noted the four polyhedra observed in these structures.

This $CeNiGe_3$ orthorhombic structure can be compared to that of the ternary germanide $Ce_3Ni_2Ge_7$ (figure 2). These two crystal structures are based on the same types of polyhedron, namely trigonal $[Ce_6]$ prisms and $[Ce_4Ge_4]$ antiprisms, which are identically stacked with $[Ce_4Ge_4]$–$[Ce_6]$–$[Ce_4Ge_4]$ sequences along the longest crystallographic axis (either a or b) and separated either by a cube $[Ge_8]$ in $CeNiGe_3$ or a cubooctahedron $[Ge_{12}]$ in $Ce_3Ni_2Ge_7$. Going from $CeNiGe_3$ to $Ce_3Ni_2Ge_7$ is then due to the insertion of an atomic plane containing Ce and Ge atoms inside the $CeNiGe_3$ $[Ge_8]$ cube. Let us notice then that if only one crystallographic site is available for Ce atoms in $CeNiGe_3$ ((4h) Wyckoff position, *Cmmm* space group), two of them are available in $Ce_3Ni_2Ge_7$ ((2d) and (4i) Wyckoff positions, *Cmmm* space group).

Using the structural parameters given in [12], we calculated the interatomic distances between a Ce atom and Ni or Ge ligands, in $CeNiGe_3$ (table 1). As the Ce atom in $CeNiGe_3$ and the (4i) Ce atom in $Ce_3Ni_2Ge_7$ [9] have the same crystallographic environment, it is worthwhile comparing these distances in the two ternary germanides. The conclusion is that $d_{Ce-Ni} = 0.3209$ nm and $d_{Ce-Ge} = 0.3183$ nm average distances in $CeNiGe_3$ at $T = 300$ K are smaller than those existing around the equivalent Ce atom in $Ce_3Ni_2Ge_7$, which are respectively equal to 0.3320 and 0.3211 nm at $T = 300$ K.

Figure 3 shows an HREM image taken along the [001] zone-axis direction. This image which is representative of the whole specimen is consistent with the diffraction patterns (figure 1). No extra reflections or diffusion were observed in the reciprocal lattice; no extended

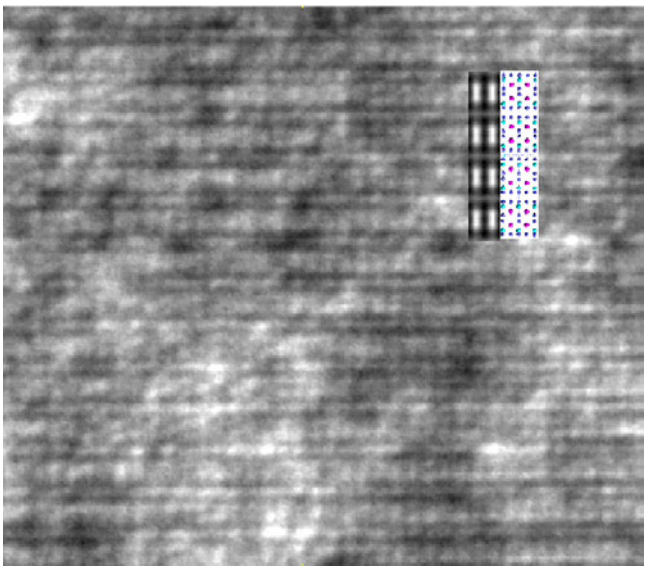

Figure 3. Characteristic HREM experimental image of $CeNiGe_3$ in the *ab*-plane, with a calculated image in the inset.

(This figure is in colour only in the electronic version)

Table 1. Interatomic distances at 300 K (<0.450 nm) around Ce atom in $CeNiGe_3$.

Ce–2Ce	0.41684(1)	Ce–4Ni	0.3209(2)
Ce–2Ce	0.41351(1)	Ce–2Ge(1)	0.3265(3)
Ce–2Ce	0.4127(4)	Ce–4Ge(1)	0.3121(1)
		Ce–2Ge(2)	0.3206(3)
		Ce–2Ge(3)	0.3200(3)

defects are detected in the image. The absence of any local defect should be emphasized. The experimental image has been compared with a simulated one obtained by a multislice approach with $CeNiGe_3$ structure. This calculated image together with the projected $CeNiGe_3$ crystal structure are inset in figure 3; the fit between experimental and calculated images confirms the $CeNiGe_3$ structural determination in [12]. The absence of any defect indicates that there is no deviation from the stoichiometry up to the nanometre scale.

3.2. Electrical and magnetic properties

Figure 4 shows the thermal dependence of the reduced electrical resistivity $\rho(T)/\rho$ (240 K) for $CeNiGe_3$. (*Due to the presence of microcracks in this polycrystalline sample, absolute values of* $\rho(T)$*could not be determined accurately*.) This curve, comparable with that observed for $CeIrGe_3$ [4], is typical of an ordered Kondo system showing the presence of the crystal field splitting of the 4f(Ce) electron. The resistivity decreases slowly with decreasing temperature from 240 to 90 K, below which it starts to decrease rapidly exhibiting a downward curvature resulting from the crystalline field effect. Below 14 K, $\rho(T)/\rho(240\,\mathrm{K})$ tends towards saturation then decreases suddenly around 5.5 K down to 0.03 (inset of figure 4), which is a rather low value, indicating a low residual resistivity and therefore good sample quality. Below 3 K, it follows a T^3 law with no signs of the conventional T^2 Fermi liquid behaviour, possibly

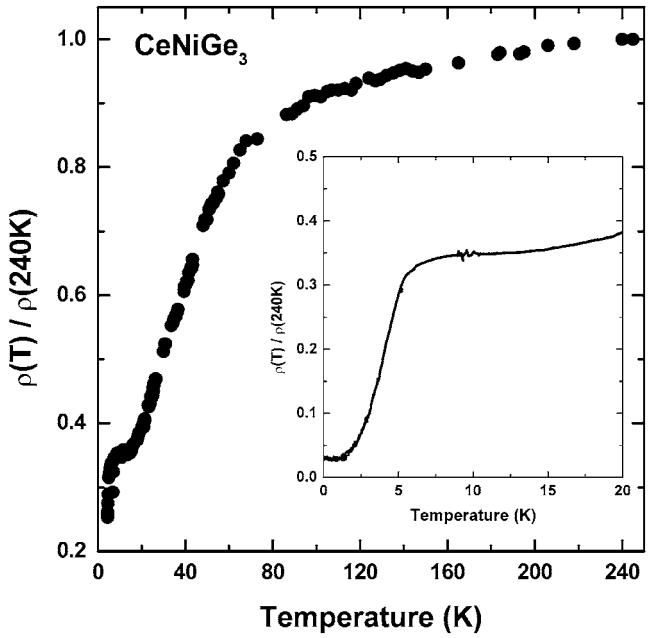

Figure 4. Temperature dependence of the reduced electrical resistivity of $CeNiGe_3$ (inset for $T \leqslant 20$ K).

masked by complex magnetic scattering processes related to the changes in the magnetic structure discussed below in connection with neutron diffraction experiments.

Above 80 K, the magnetic susceptibility of $CeNiGe_3$ follows a Curie–Weiss law characterized by $\theta_p = -12(1)$ K and $\mu_{eff} = 2.58(5)\ \mu_B$/Ce (theoretical value for Ce^{3+} ion equal to 2.56 μ_B) as paramagnetic Curie temperature and effective magnetic moment. These values are in good agreement with those previously determined by other authors [6]. Our dc-magnetization measurements at low applied magnetic fields [12] suggest that $CeNiGe_3$ is antiferromagnetically ordered below $T_N = 5.5(2)$ K. In order to obtain more information on this ordering, we have measured at various frequencies the ac-magnetic susceptibility of this ternary germanide. The ac-susceptibility measurements at low temperature are shown in figure 5 for the in-phase component χ'. All the curves present a maximum at 5.5(2) K. No frequency dependence is observed, excluding the occurrence at low temperature of a spin-glass state for $CeNiGe_3$ as reported by Das *et al* [6]. Such a behaviour would have been indicated by the shift of the maximum of the $\chi' = f(T)$ curves to lower temperatures with decreasing frequency [16].

Figure 6 shows the influence of an applied field on $CeNiGe_3$ magnetic structure below $T_N = 5.5$ K. At $T = 2$ K, the magnetization increases linearly up to $\mu_0 H \cong 1.4$ T and then more rapidly at higher fields, suggesting an induced metamagnetic transition. At this temperature, two maxima are clearly distinguished at 1.9 and 3.3 T (inset of figure 6) in the derivative curve $\mathrm{dMag}/\mathrm{d}\mu_0 H = f(\mu_0 H)$ revealing a complex ($\mu_0 H$–T) magnetic phase diagram for this ternary germanide.

All these results confirm that $CeNiGe_3$ orders antiferromagnetically below $T_N = 5.5(2)$ K. Very recently, Pikul *et al* [17], using magnetization measurements, have indicated the same magnetic transition.

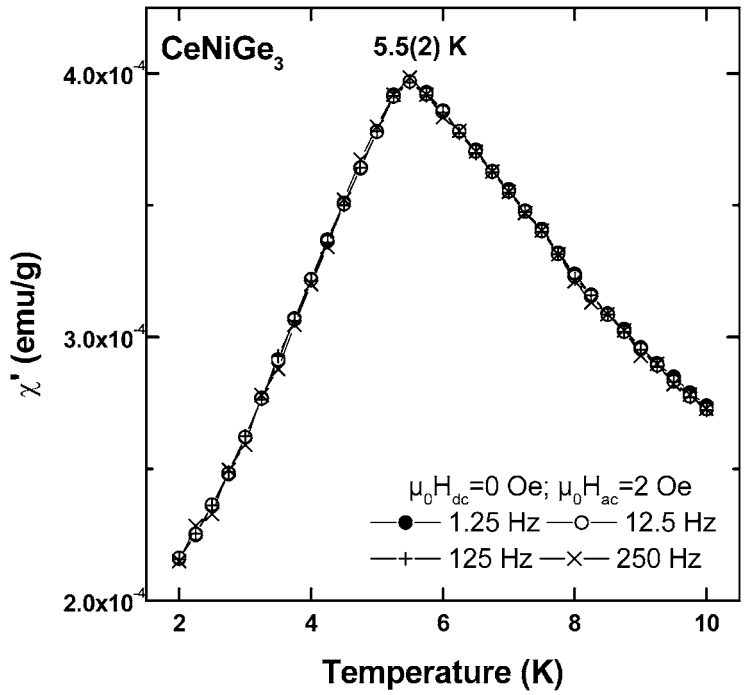

Figure 5. Temperature dependence of the in-phase component of the ac-susceptibility of $CeNiGe_3$ measured for different frequencies (dc and ac applied fields are respectively equal to 0 and 2 Oe).

3.3. Specific heat measurement

In figure 7, the specific heat data are plotted as C/T versus T. Two characteristics can be observed: a sharp peak near 5.1 K and a shoulder starting around 4.1 K (this behaviour is more visible in the curve $C/T = f(T^2)$ given in the inset of figure 7). This result is comparable to that reported on the other ternary germanide $CeCoGe_3$ [2] which also presents a peak at 21 K and a shoulder at 18 K. These measurements suggest that $CeNiGe_3$ could exhibit two magnetic transitions. Clearly, $CeNiGe_3$ shows a complex magnetic order.

The analysis of the curve $C/T = f(T^2)$ as $C/T = \gamma + \beta T^2$ yields similar γ values above 12 K and below 1.5 K, 39 and 34 mJ Ce mol^{-1} K^{-2} respectively. These values are smaller than that observed for the ternary germanide $Ce_2Ni_3Ge_5$, namely $\gamma \cong 90$ mJ Ce mol^{-1} K^{-2} [10]. It should also be noticed for $CeNiGe_3$ that the magnetic entropy at the magnetic transition $\cong$5.1 K is only 65% of $R \ln 2 = 5.76$ J mol^{-1} K^{-1} corresponding to a doublet ground state. This behaviour can be interpreted as a consequence of the presence of the Kondo interaction in this ternary germanide. Similar reduction of the magnetic entropy is also detected for $Ce_2Ni_3Ge_5$ [10].

3.4. Magnetic structure

NPD patterns have been registered for $CeNiGe_3$ at low temperatures, between 1.5 and 11.9 K (figure 8). At 11.9 K, above the magnetic transition temperature T_N, only nuclear diffraction peaks are present. The lattice parameters are $a = 2.183\,38(8)$ nm, $b = 0.413\,64(2)$ nm and $c = 0.416\,54(2)$ nm.

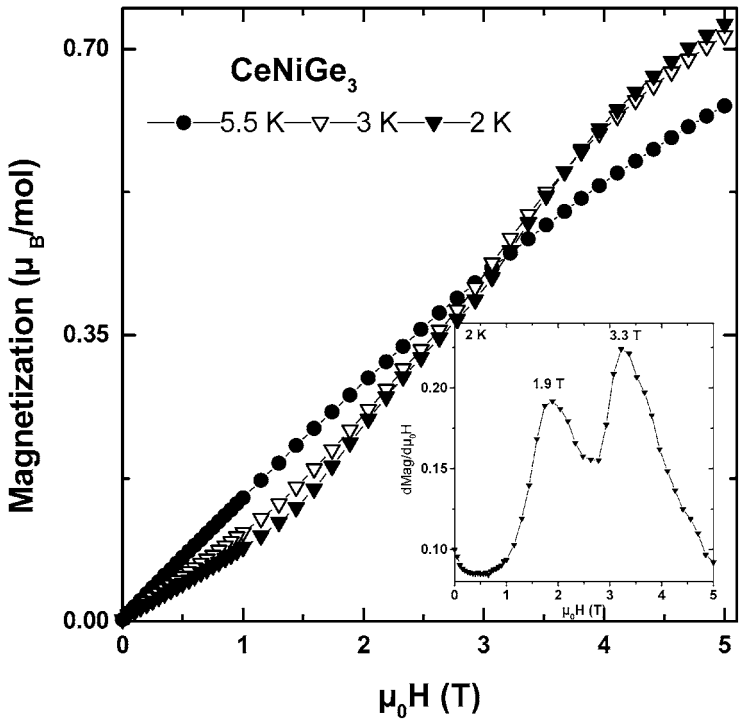

Figure 6. Field dependence of the magnetization of $CeNiGe_3$ measured at different temperatures (the inset shows the variation at 2 K of the derivative curve $\mathrm{dMag}/\mathrm{d}\mu_0 H$).

At 1.5 K, additional peaks of magnetic origin are detected, with rather weak intensities. Two series of magnetic reflections are present, which appear at two different temperatures and exhibit different thermal variations. Just one magnetic Bragg peak belongs to the first series: this peak appears at $2\theta = 6.37°$ (figure 8), and is labelled as $\underline{1\,0\,0}$; this first magnetic mode is characterized by a magnetic unit cell identical to the chemical unit cell, and a propagation vector $\boldsymbol{k}_1 = (100)$. Reflections in the second series are referenced as $0\,0\,0^{\pm}$, $2\,0\,0^{\pm}$, $1\,1\,0^{-}$, $3\,1\,0^{-}$, ... and associated with the incommensurate $\boldsymbol{k}_2 = (0\,0.409(1)\,1/2)$ propagation vector. Below the magnetic transition temperatures, no change is observed for $\boldsymbol{k}_1$ and $\boldsymbol{k}_2$ component values as a function of temperature.

Figure 9 shows the thermal dependence of the most intense magnetic Bragg peak reflections associated with each propagation vector, $1\,0\,0$ ($\boldsymbol{k}_1$) and $0\,0\,0^{\pm}$ ($\boldsymbol{k}_2$): two magnetic transitions are then evidenced, at $T_{N1} = 5.9(2)$ and $T_{N2} = 5.0(2)$ K. If the $\boldsymbol{k}_2(000^{\pm})$ magnetic peak appears at T_{N2} and then shows a regular increase of intensity down to 1.5 K, the $1\,0\,0$ magnetic intensity variation is more surprising, passing through a maximum near 4.1 K. The magnetic structures associated with $\boldsymbol{k}_1$ and $\boldsymbol{k}_2$ then have correlated thermal behaviours. Let us now analyse these magnetic structures.

3.4.1. Commensurate magnetic structure ($\boldsymbol{k}_1$). At 5 K, only one magnetic peak is observed, the indices of which, $1\,0\,0$, obey the selection rule $h + k = 2n + 1$. This condition yields non-identical magnetic moments for Ce atoms separated by the C translation $[1/2\ 1/2\ 0]$. If these magnetic moments are parallel and do have the same absolute value, then they must be opposite. As the positional parameter x_{Ce} is nearly identical to $1/6$ [12], and

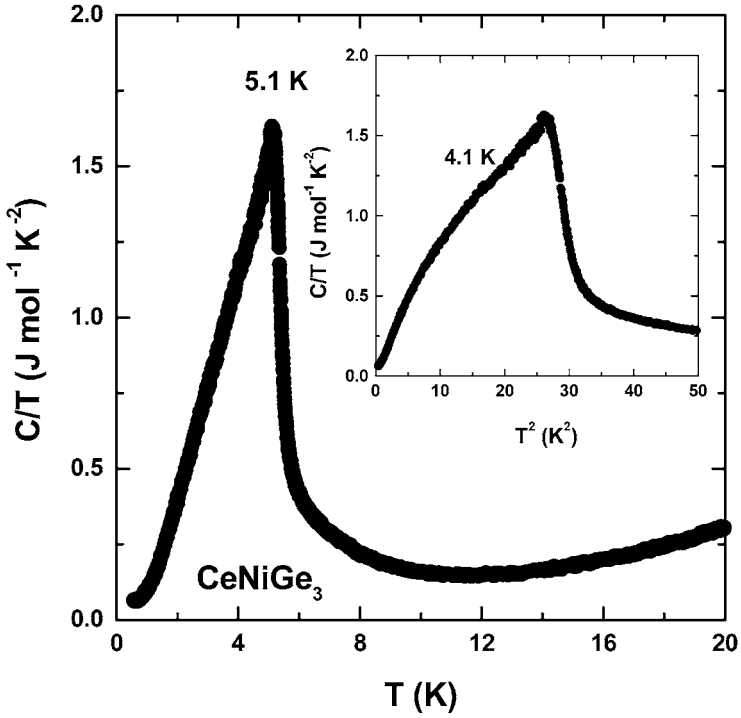

Figure 7. Temperature dependence of the specific heat C divided by temperature T for $CeNiGe_3$ (inset curve C/T versus T^2).

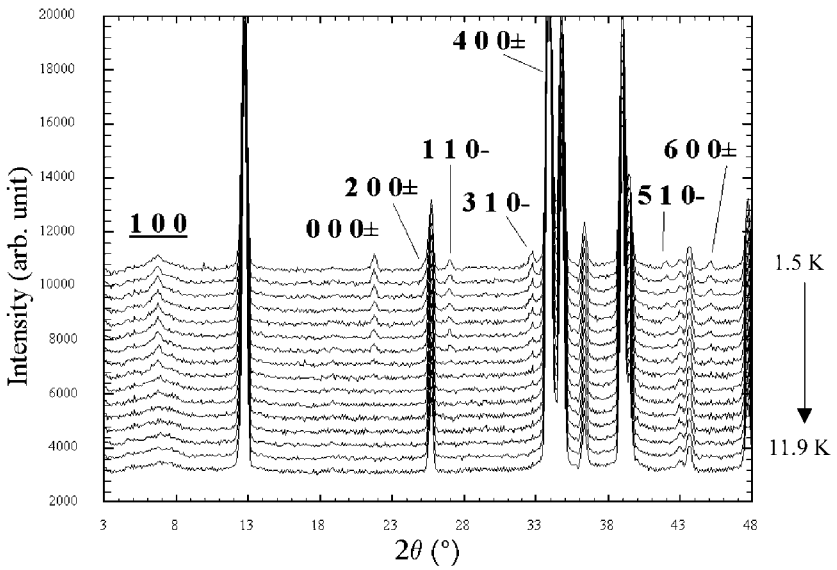

Figure 8. NPD pattern ($\lambda = 0.2426$ nm) of $CeNiGe_3$ from 1.5 to 11.9 K (only magnetic reflections are indexed). The first magnetic reflection $\underline{1\,0\,0}$ is indexed on the basis of the chemical unit cell and the others are associated with the propagation vector $k_2 = (0\ 0.409(1)\ 1/2)$.

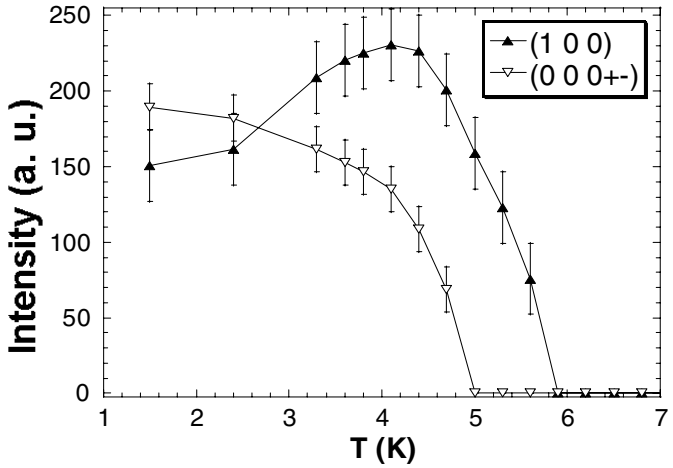

Figure 9. Temperature dependence of the intensity of two magnetic reflections of $CeNiGe_3$: 1 0 0 and $0\,0\,0^{\pm}$ respectively associated with $\boldsymbol{k}_1 = (100)$ and $\boldsymbol{k}_2 = (0\,0.409(1)\,1/2)$ propagation vectors.

no 3 0 0 magnetic reflection is present (*this should have been observed at* $2\theta = 19.91°$ (figure 8)), the sequence '$++--$' is obtained for magnetic moments of Ce I [x_{Ce} 0 1/2], Ce II [$1/2 - x_{Ce}$ 1/2 1/2], Ce III [$1/2 + x_{Ce}$ 1/2 1/2] and Ce IV [$1 - x_{Ce}$ 0 1/2] atoms in the nuclear unit cell. Bertaut's representation analysis [18] applied to *Cmmm* space group, (4h) Wyckoff position and $\boldsymbol{k}_1 = (100)$ only yields basis vectors parallel to the *a*-, *b*- or *c*-axis. So, in the present case, the Ce magnetic moments are either directed along the *b*- or *c*-axis, but we cannot draw conclusions about their direction with only the 1 0 0 magnetic peak observed. Comparison between experimental and calculated data (reliability factor $R_M = 16\%$) leads to $M_{Ce} = 0.22(2)\ \mu_B$/Ce at 5 K. This magnetic structure is presented in figure 10(a), with Ce magnetic moments parallel to either the *b*- or *c*-axis (figure 10(a)). In both cases, the Ce magnetic moments form ferromagnetic (100)-planes. At 5 K, the coherence length associated with this commensurate structure is 10(5) nm.

The commensurate magnetic structure of $CeNiGe_3$ can be compared to that of $Ce_3Ni_2Ge_7$ (figure 11). Let us recall that in $Ce_3Ni_2Ge_7$, the Ce1 atoms occupying the [Ge_{12}] cubo-octahedron do not carry any ordered magnetic moment [9]. As a consequence, these two magnetic structures are identical: they can be described by antiferromagnetic stacking along the *a*-axis ($CeNiGe_3$) or *b*-axis ($Ce_3Ni_2Ge_7$) of layers of ferromagnetic trigonal prisms [Ce_6]. Similar ferromagnetic coupling within [Ce_6] prisms is commonly observed in intermetallics based on cerium, for instance in the $CeNi_{0.84}Sn_2$ ternary stannide (ferromagnetic structure) [19].

3.4.2. Incommensurate magnetic structure ($\boldsymbol{k}_2$). As already mentioned, two different propagation vectors for magnetic structures (commensurate $\boldsymbol{k}_1$ and incommensurate $\boldsymbol{k}_2$) are observed at 1.5 K for $CeNiGe_3$. Two assumptions can then be made (and NPD is unable to decide between these two): either the two magnetic structures are associated with the whole volume of the sample or each of these magnetic arrangements occupies a partial volume in the sample. We select the partial volume assumption, from the criterion of identical Ce magnetic moment values in the two magnetic structures. The best fit between experimental and calculated neutron diffraction patterns (difference pattern 1.5–11.9 K) indicates that

(i) the magnetic structure associated with the $\boldsymbol{k}_2$ propagation vector is a helicoidal magnetic structure with Ce magnetic moments in the (*ab*)-plane;

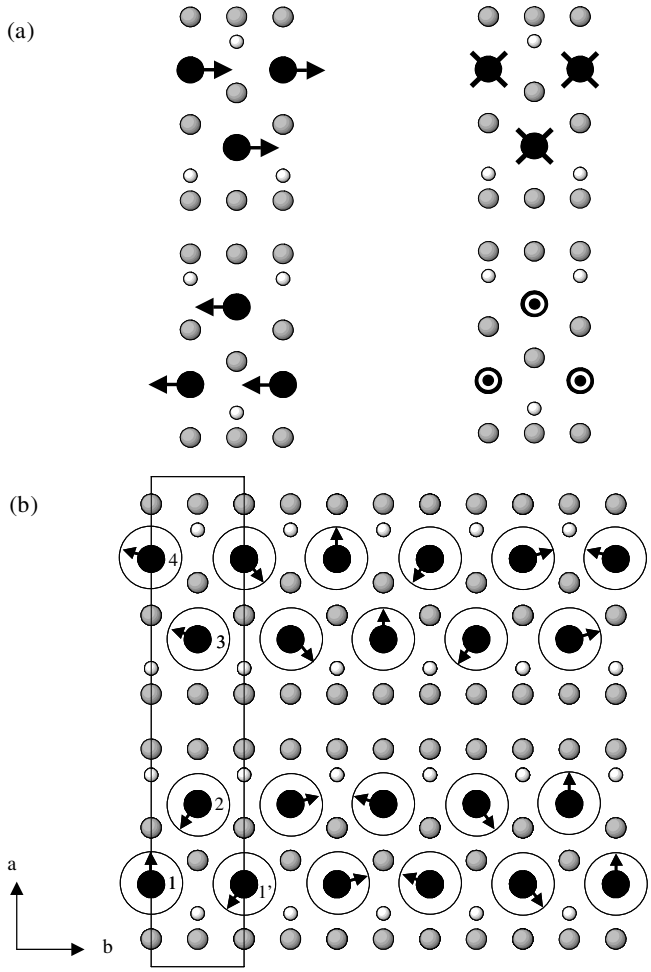

Figure 10. Projection onto the 001-plane of the magnetic structures of $CeNiGe_3$ (Ce, Ge and Ni are respectively represented by large black, medium grey and small white circles, the Ce magnetic moments are represented by black arrows): (a) the two possibilities for the commensurate structure and (b) the incommensurate helicoidal structure (the helix plane is given by a circle).

(ii) within the 'partial volume' assumption and identical values for commensurate and incommensurate magnetic moments, the value of the Ce magnetic moment is 0.8(2) μ_B. At 1.5 K, the respective volumes for commensurate and incommensurate magnetic phases are $V_1 = 7(5)\%$ and $V_2 = 93(5)\%$.

At $T = 1.5$ K, the coherence lengths associated with these two magnetic structures are 10(5) and 75(15) nm for the commensurate and the incommensurate magnetic structures respectively. These values indicate that the incommensurate magnetic structure is more stable in this temperature range. Moreover, between 4.7 K $< T_{N2}$ and 1.5 K, the volume for the incommensurate phase increases from 79(5) to 93(5)%.

The $CeNiGe_3$ incommensurate helicoidal magnetic structure is drawn in figure 10(b). The turning angle between the Ce1 atom and its equivalent Ce 1′ in the next nearest unit cell along the b-axis is close to 144° ($2\pi k_{2,y}$ with $k_y = 0.40$). Due to the component $k_{2Z} = 1/2$ of

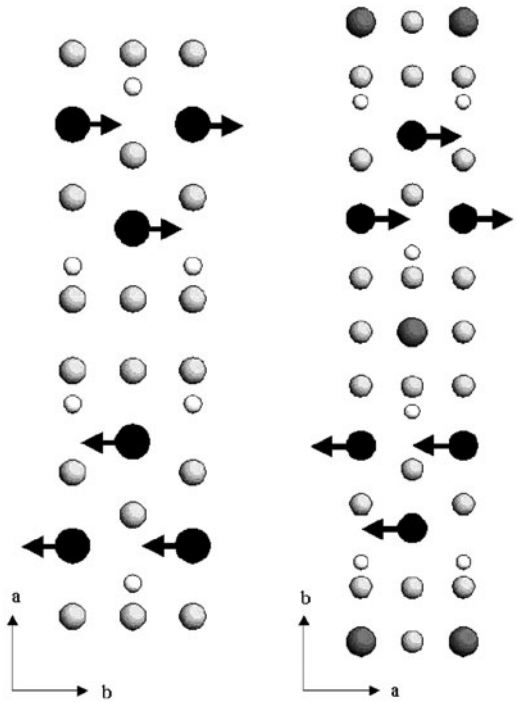

Figure 11. Comparison between the commensurate magnetic structure of $CeNiGe_3$ (left) and that of $Ce_3Ni_2Ge_7$ (right). Ce1, Ce2 or Ce, Ge and Ni atoms are respectively represented by large grey, large black, medium grey and small white circles.

the k_2 propagation vector, all Ce magnetic moments turn over 180° between neighbouring (001)-planes.

Analysing the $CeNiGe_3$ incommensurate magnetic structure in comparison to $CeNiGe_3$ commensurate magnetic structure, different coupling schemes are to be assumed:

(i) along the *c*-axis, all the Ce–Ce couplings are antiferromagnetic in the incommensurate case instead of being ferromagnetic (commensurate case);

(ii) within the (*ab*)-basal plane the coupling between nearest Ce neighbours is no longer ferromagnetic. The magnetic moments are then not parallel and this situation is a 'classical' compromise adopted when antiferromagnetic coupling is present in a triangular network.

This type of magnetic behaviour, i.e. simultaneous existence of commensurate and incommensurate magnetic structures, has already been observed in $CeNi_{0.84}Sn_2$, a ternary stannide with $CeNiSi_2$-type structure, including $[Ce_6]$ trigonal prisms and $[Ce_4Ge_4]$ antiprisms as in $CeNiGe_3$. At 1.5 K $CeNi_{0.84}Sn_2$ exhibits two coexisting magnetic phases: the first is ferromagnetic; the other is an antiferromagnetic modulated phase [19]. This behaviour has been attributed to the occurrence of concentration fluctuations associated with the Ni deficiency of this ternary stannide. As no similar defects in $CeNiGe_3$ are observed via TEM investigation on the studied sample, this interpretation cannot be retained in the present case. Perhaps, the presence of germanium as an impurity phase in our sample could slow down the advance of the incommensurate phase at low temperature.

Another interesting magnetic property in $CeNiGe_3$ is that the value of M_{Ce} is only 0.8(2) μ_B, a reduced magnetic moment in comparison to $M_{Ce} = 1.98(2)\ \mu_B$ for 'magnetic' Ce atoms in $Ce_3Ni_2Ge_7$ which have a similar crystallographic environment. But as the average interatomic distances d_{Ce-Ni} and d_{Ce-Ge} are smaller in $CeNiGe_3$, the mixing of 4f(Ce) orbitals with Ni and Ge ligand orbitals may be favoured in $CeNiGe_3$, a higher orbital hybridization inducing a 4f(Ce)-state broadening and consequently a reduction of the Ce magnetic moment.

4. Conclusion

The crystal structure of $CeNiGe_3$ has been solved using TEM investigation and NPD (orthorhombic $SmNiGe_3$-type structure). Two magnetic transitions have been evidenced by NPD and specific heat measurements, at $T_{N1} = 5.9(2)$ K and $T_{N2} = 5.0(2)$ K (NPD result). T_{N1} is associated with a commensurate collinear antiferromagnetic structure, with $\boldsymbol{k}_1 = (100)$ propagation vector. This magnetic structure is described by ferromagnetic $[Ce_6]$ trigonal prisms, with an antiferromagnetic arrangement of the $[Ce_6]$ layers. The Ce magnetic moments are most probably directed along the $\boldsymbol{b}$-axis. A similar ferromagnetic coupling within trigonal prisms is also found in the other ternary germanide $Ce_3Ni_2Ge_7$. T_{N2} is associated with an incommensurate antiferromagnetic structure, with $\boldsymbol{k}_2 = (0\ 0.409(1)\ 1/2)$ propagation vector and magnetic moments within (ab)-plane. In fact, below T_{N2}, the two magnetic structures coexist, with a thermally dependent relative weight, the incommensurate structure being highly preponderant at 1.5 K. Heat capacity measurements show a clear peak at the magnetic transition with lowest critical temperature, which masks a possible contribution from the transition with highest critical temperature. An anomalous bump appears at around 4.1 K, where the intensity of the commensurate (100) magnetic reflection decreases (figure 9), reflecting the complex behaviour of the magnetic properties of this ternary germanide. Magnetic measurements only revealed one magnetic transition at 5.5(2) K, a temperature between T_{N1} and T_{N2} evidenced by NPD. (*In other words, the magnetization measurements detect only an average ordering magnetic temperature*.) The Ce magnetic moment at 1.5 K is 0.8(2) μ_B and $CeNiGe_3$ can be considered as a magnetically ordered Kondo system, as suggested already by electrical resistivity measurements.

As a conclusion, the magnetic behaviour of $CeNiGe_3$ is rather complex, with competing ferromagnetic and antiferromagnetic interactions within $[Ce_6]$ trigonal prisms. The reason for such a competition is not clear at the present time.

References

[1] Yamamoto H, Ishikawa M, Hasegawa K and Sakurai J 1995 *Phys. Rev.* B **52** 10136
[2] Pecharsky V K, Hyun O B and Gschneidner K A Jr 1993 *Phys. Rev.* B **47** 11839
[3] Eom D, Ishikawa M, Kitagawa J and Takeda N 1998 *J. Phys. Soc. Japan* **67** 2495
[4] Muro Y, Eom D, Takeda N and Ishikawa M 1998 *J. Phys. Soc. Japan* **67** 3601
[5] Muro Y, Eom D H, Takeda N, Ishikawa M, Kanai K, Watenabe M and Shin S 1999 *Physica* B **259–261** 1114
[6] Das A, Menon L, Nigam A K and Malik S K 1997 *Physica* B **230–232** 165
[7] Salamakha P, Konyk M, Sologub O and Bodak O 1996 *J. Alloys Compounds* **236** 206
[8] Chevalier B and Etourneau J 1999 *J. Magn. Magn. Mater.* **196/197** 880
[9] Durivault L, Bourée F, Chevalier B, André G, Etourneau J and Isnard O 2001 *J. Magn. Magn. Mater.* **232** 139
[10] Hossain Z, Hamashima S, Umeo K, Takabatake T, Geibel C and Steglich F 2000 *Phys. Rev.* B **62** 8950
[11] Durivault L, Bourée F, Chevalier B, André G and Etourneau J 2002 *J. Magn. Magn. Mater.* **246** 366
[12] Durivault L, Bourée F, Chevalier B, André G, Weill F and Etourneau J 2002 *Appl. Phys.* A at press
[13] Rodriguez-Carvajal J 1990 *Satellite Mtg 15th Congr. IUCr on Powder Diffraction (Toulouse, 1990)* p 127

[14] Sears V F 1992 *Neutron News* **3** 26
[15] Freeman A J and Desclaux J P 1979 *J. Magn. Magn. Mater.* **12** 11
[16] Mydosh J A 1993 *Spin Glass: an Experimental Introduction* (London: Taylor and Francis)
[17] Pikul A P, Kaczorowski D and Rogl P 2002 *Physica* B **312/313** 422
[18] Bertaut E F 1968 *Acta Crystallogr.* A **24** 217
[19] Schobinger-Papamantellos P, Rodriguez-Carvajal J, Prokes K and Buschow K H J 1996 *J. Phys.: Condens. Matter* **8** 8635